Stable, Accurate and Efficient Interface Procedures for Viscous Problems

Jing Gong and Jan Nordström

April 6, 2006

Abstract

In this paper we investigate and study several different interface procedures for finite difference methods applied to viscous problems. The analysis show that stable, accurate and efficient interface procedures can be obtained. The analysis also show that only minor differences of the various methods exist.

keywords high order finite difference methods; numerical stability; accuracy; interface conditions; summation-by-parts

1 Introduction

In computational aerodynamics, the computational domain is often for efficiency and mesh generation reasons divided into multiple blocks. Stable and accurate coupling at the block interfaces is very important since information often have to travel relatively long distances during long times. When advection is the dominant transport process, most numerical procedures introduce non-physical oscillations and excessive numerical diffusion.

The development of numerical schemes that overcome the problems above is an ongoing challenge. High order finite difference methods provide an efficient approach when high resolution is essential. Strictly stable and accurate high order finite difference methods for both hyperbolic, parabolic and incompletely parabolic problems were derived in [3], [8], [9], [11]–[13], [15]-[17], [20]. These methods employ so called Summation-by-Parts (SBP) operators and the Simultaneous Approximation Term (SAT) procedure, see [2], [3], [11], [14], [20], [21]. The SAT procedure is a penalty method where the penalty parameters are determined by stability requirements.

In order to speed up convergence to steady state it is essential that the spectral radius of the numerical scheme is minimal. It is also important to have operators with a small spectral radius such that a large time step may be used for explicit time stepping, see [22].

In [3], [13] various versions of the SAT method in multiple domains was presented. We will continue this investigation and study several different interface procedures which maintain stability, conservation, and accuracy in multiple domains. Also, we consider the size of the spectral radius since that influence the efficiency of the explicit time integration. Finally we investigate the reflexion properties of the different interface treatments. The SAT formulation can easily be extended to several space dimensions and to complicated boundary conditions (see [13], [15], [16], [17]). For clarity, we consider the one-dimensional scalar advection-diffusion equation in this paper.

In Section 2 and 3 we derive stable conditions for the continuous and semi-discrete problems respectively. We also derive the penalty formulation for multiple domains and obtain sufficient conditions for stability of the semi-discrete form. We study the size and location of the eigenvalues in Section 4. In Section 5 we perform numerical experiments and compare the efficiency of the interface procedures. Conclusions are drawn in Section 6.

2 The continuous problem

Consider the model problem in one space dimension,

$$\begin{aligned}
u_t + au_x &= \varepsilon u_{xx} + F, && 0 \le x \le 1, \quad t > 0, && \text{(1a)}\\
\alpha u(0,t) + \beta u_x(0,t) &= g^L(t), && t \ge 0, && \text{(1b)}\\
\gamma u(1,t) + \delta u_x(1,t) &= g^R(t), && t \ge 0, && \text{(1c)}\\
u(x,0) &= f(x), && 0 \le x \le 1, && \text{(1d)}
\end{aligned}$$

where a, $\varepsilon > 0$ and $\varepsilon \ll a$. In most cases we use $F = 0$.

Let the inner product for real valued functions $a, b \in L[0,1]$ be defined by $(a,b) = \int_0^1 ab\, dx$ and the corresponding norm $\|a\|^2 = (a,a)$. Applying the energy method to (1) with $F=0$ yields

$$
\begin{aligned}
\frac{d}{dt}(\|u\|^2) + 2\varepsilon\|u_x\|^2 = & \left(a + \frac{2\alpha}{\beta}\varepsilon\right)\left(u(0,t) - \frac{\varepsilon}{\beta}\frac{1}{a+\frac{2\alpha}{\beta}\varepsilon}g^L(t)\right)^2 \\
& -\left(a + \frac{2\gamma}{\delta}\varepsilon\right)\left(u(1,t) - \frac{\varepsilon}{\delta}\frac{1}{a+\frac{2\gamma}{\delta}\varepsilon}g^R(t)\right)^2 \\
& -\left(\frac{\varepsilon}{\beta}\right)^2\left(\frac{1}{a+\frac{2\alpha}{\beta}\varepsilon}\right)g^L(t)^2 \\
& +\left(\frac{\varepsilon}{\delta}\right)^2\left(\frac{1}{a+\frac{2\gamma}{\delta}\varepsilon}\right)g^R(t)^2.
\end{aligned}
\tag{2}
$$

Hence an energy estimate is obtained if

$$
a + \frac{2\alpha}{\beta}\varepsilon < 0 \quad \text{and} \quad a + \frac{2\gamma}{\delta}\varepsilon > 0. \tag{3}
$$

We have proved the following proposition.

Proposition 2.1 *With condition (3) satisfied, the problem (1) is strongly well posed.*

Remark: When the solution can be estimated in terms of all types of data, the problem (1) is called strongly well posed, see [7] for more details.

3 The semi-discrete problem

3.1 Single domain

Consider the problem (1) discretized on the single domain $[0,1]$ with a uniform mesh of $(N+1)$ points. The vector $\mathbf{u} = [u_0, u_1, \ldots, u_N]$ is the discrete approximation of u. The discrete approximation of u at the grid point i is denoted u_i. $\mathbf{u}_x$ and $\mathbf{u}_{xx}$ are the approximations of u_x and u_{xx}, respectively. By using the SBP operators constructed in [8] and [20] we have

$$
\begin{aligned}
\mathbf{u}_x &= D_1\mathbf{u} = P^{-1}Q\mathbf{u}, \\
\mathbf{u}_{xx} &= D_{2n}\mathbf{u} = D_1(D_1\mathbf{u}) = \left(P^{-1}Q\right)^2\mathbf{u}, \quad \text{or} \\
\mathbf{u}_{xx} &= D_{2c}\mathbf{u} = P^{-1}(-A+BS)\mathbf{u},
\end{aligned}
\tag{4}
$$

where $A + A^T \geq 0$. P is a symmetric positive definite matrix and Q is an almost skew-symmetric matrix that satisfies

$$
Q + Q^T = B = \mathrm{diag}([-1, 0, \ldots, 0, 1]).
$$

Both operators D_{2n} and D_{2c} satisfy the second derivative SBP property, see (6) below. Moreover, D_{2c} is a difference operator with minimum bandwidth. The operator S has the form (see [11]),

$$S = \begin{bmatrix} -s_1 & \cdots & -s_r & 0 & \cdots \\ & 1 & & & \\ & & \ddots & & \\ & & & 1 & \\ \cdots & 0 & s_r & \cdots & s_1 \end{bmatrix}.$$

The first and last row of S approximates the first derivative at the two boundaries, respectively. For simplicity, we denote

$$(D_{1B}\mathbf{u})_0 = \begin{cases} (D_1\mathbf{u})_0, & \text{if } D_{2n} \text{ used,} \\ (S\mathbf{u})_0, & \text{if } D_{2c} \text{ used,} \end{cases} \quad (D_{1B}\mathbf{u})_N = \begin{cases} (D_1\mathbf{u})_N, & \text{if } D_{2n} \text{ used,} \\ (S\mathbf{u})_N, & \text{if } D_{2c} \text{ used.} \end{cases}$$

As a result, the semi-discrete approximation of (1) can be written

$$\begin{aligned} \mathbf{u}_t + aD_1\mathbf{u} =& \varepsilon D_2\mathbf{u} + \tau^L P^{-1}\mathbf{e}_0\big[\alpha u_0 + \beta(D_{1B}\mathbf{u})_0 - g^L\big] && \text{(5a)} \\ & + \tau^R P^{-1}\mathbf{e}_N\big[\gamma u_N + \delta(D_{1B}\mathbf{u})_N - g^R\big], \\ \mathbf{u}(t=0) =& f. && \text{(5b)} \end{aligned}$$

In (5), D_2 is either D_{2n} or D_{2c}. The SAT treatment (see [2], [3], [11], [14], [20], [21]) is used to implement the boundary condition and the coefficients τ^L and τ^R are chosen to given a stable scheme. The vectors $\mathbf{e}_0 = [1, 0, \dots, 0]^T$ and $\mathbf{e}_N = [0, 0, \dots, 1]^T$ are used to pick up the boundary points.

We define a discrete inner product and norm for the gridfunctions by

$$(\mathbf{u}, \mathbf{v})_P = \mathbf{u}^T P\mathbf{v} \quad \text{and} \quad \|\mathbf{u}\|_P^2 = (\mathbf{u}, \mathbf{u})_P = \mathbf{u}^T P\mathbf{u}.$$

and note that

$$\begin{aligned} \mathbf{u}^T\big[PD_{2n} + (PD_{2n})^T\big]\mathbf{u} &= \|D_1\mathbf{u}\|_P^2 - u_0(D_{1B}\mathbf{u})_0 + u_N(D_{1B}\mathbf{u})_N, \\ \mathbf{u}^T\big[PD_{2c} + (PD_{2c})^T\big]\mathbf{u} &= (\mathbf{u}, \mathbf{u})_{A+A^T} - u_0(D_{1B}\mathbf{u})_0 + u_N(D_{1B}\mathbf{u})_N. \end{aligned} \tag{6}$$

For more details on the finite difference approximations of second derivatives, see [11].

We apply the energy method by multiplying (5a) by $\mathbf{u}^T P$, and adding the transpose. This yields,

$$
\begin{aligned}
\frac{d}{dt}\left(\|u\|_P^2\right) + 2\varepsilon \mathrm{Diss} =& a u_0^2 - a u_N^2 - 2\varepsilon u_0 (D_{1B}\mathbf{u})_0 + 2\varepsilon u_N (D_{1B}\mathbf{u})_N \\
&+2\tau^L \alpha u_0^2 + 2\tau^L \beta u_0 (D_{1B}\mathbf{u})_0 - 2\tau^L u_0 g^L \\
&+2\tau^R \gamma u_N^2 + 2\tau^R \delta u_N (D_{1B}\mathbf{u})_N - 2\tau^R u_N g^R \\
=& (a + 2\tau^L\alpha)\left(u_0 - \frac{\tau^L}{a+2\tau^L\alpha} g^L\right)^2 \\
&-(a - 2\tau^R\gamma)\left(u_N - \frac{\tau^R}{a-2\tau^R\gamma} g^R\right)^2 \\
&-\frac{{\tau^L}^2}{a+2\tau^L\alpha} {g^L}^2 + \frac{{\tau^R}^2}{a-2\tau^R\gamma} {g^R}^2 \\
&-\underbrace{2(\varepsilon - \tau^L\beta) u_0 (D_{1B}\mathbf{u})_0}_{(I)} \\
&+\underbrace{2(\varepsilon + \tau^R\delta) u_N (D_{1B}\mathbf{u})_N}_{(II)},
\end{aligned}
\tag{7}
$$

where Diss represents $\|D_1\mathbf{u}\|_P^2$ if D_{2n} is used and $(\mathbf{u},\mathbf{u})_{A+A^T}$ if D_{2c} is used.

For canceling the terms (I) and (II) in equation (7), we require

$$
\tau^L = \frac{\varepsilon}{\beta} \quad \text{and} \quad \tau^R = -\frac{\varepsilon}{\delta}. \tag{8}
$$

Substituting (8) into (7) we have

$$
\begin{aligned}
\frac{d}{dt}\left(\|u\|_P^2\right) + 2\varepsilon \mathrm{Diss} =& \left(a + \frac{2\alpha}{\beta}\varepsilon\right)\left(u_0 - \frac{\varepsilon}{\beta}\frac{1}{a+\frac{2\alpha}{\beta}\varepsilon} g^L\right)^2 \\
&-\left(a + \frac{2\gamma}{\delta}\varepsilon\right)\left(u_N - \frac{\varepsilon}{\delta}\frac{1}{a+\frac{2\gamma}{\delta}\varepsilon} g^R\right)^2 \\
&-\left(\frac{\varepsilon}{\beta}\right)^2\left(\frac{1}{a+\frac{2\alpha}{\beta}\varepsilon}\right){g^L}^2 + \left(\frac{\varepsilon}{\delta}\right)^2\left(\frac{1}{a+\frac{2\gamma}{\delta}\varepsilon}\right){g^R}^2.
\end{aligned}
\tag{9}
$$

We have obtained the following result.

Proposition 3.1 *If condition (3) for well-posedness and (8) are satisfied, the approximation (5) is strongly stable.*

Remark: When the solution can be estimated in terms of all types of data, the problem is called strongly stable, see [7] for more details.

Remark: The estimate (9) is completely similar to the continuous estimate (2).

3.2 Multiple domains and interface conditions

Without loss of generality, we consider a computational domain which consists of two subdomains. The unknown on the left subdomain is denoted by u and on the right subdomain by v, respectively. The same technique described in the previous section is used here to discretize both u and v. The corresponding notations are also modified by adding superscripts ^{L} and ^{R} in order to identify the left and right subdomains.

Since the outer boundary treatment has been already discussed, we will only focus on the interface treatment. The coupling of $\mathbf{u}$ and $\mathbf{v}$ as well as the first derivatives $D_1^L\mathbf{u}$ and $D_1^R\mathbf{v}$ at the interface will be treated by using the various forms of the SAT technique.

3.2.1 The Baumann-Oden method

In this method (first proposed in [1]), the semi-discrete approximation of (1) is given by

$$\begin{aligned}\mathbf{u}_t + aD_1^L\mathbf{u} = \varepsilon D_2^L\mathbf{u} + &\sigma_1^L(P^L)^{-1}\mathbf{e}_N^L(u_N - v_0) + \\ &\sigma_2^L(P^L)^{-1}\mathbf{e}_N^L\left[(D_{1B}^L\mathbf{u})_N - (D_{1B}^R\mathbf{v})_0\right] + \\ &\sigma_3^L(P^L)^{-1}(D_{1B}^L)^T\mathbf{e}_N^L(u_N - v_0) + \mathrm{BT}^L,\end{aligned} \tag{10a}$$

on the left subdomain, and

$$\begin{aligned}\mathbf{v}_t + aD_1^R\mathbf{v} = \varepsilon D_2^R\mathbf{v} + &\sigma_1^R(P^R)^{-1}\mathbf{e}_0^R(v_0 - u_N) + \\ &\sigma_2^R(P^R)^{-1}\mathbf{e}_0^R\left[(D_{1B}^R\mathbf{v})_0 - (D_{1B}^L\mathbf{u})_N\right] + \\ &\sigma_3^R(P^R)^{-1}(D_{1B}^R)^T\mathbf{e}_0^R(v_0 - u_N) + \mathrm{BT}^R,\end{aligned} \tag{10b}$$

on the right subdomain. The coefficients σ_1^L, σ_2^L, σ_3^L, σ_1^R, σ_2^R, σ_3^R will be determined by stability considerations. D_2^L represents D_{2n}^L or D_{2c}^L and D_2^R represents D_{2n}^R or D_{2c}^R. BT^L and BT^R are introduced to represent the stable left and right boundary terms respectively.

Apply the energy method by multiplying (10a) and (10b) with $\mathbf{u}^TP^L$ and $\mathbf{v}^TP^R$ respectively. This leads to

$$\begin{aligned}\mathbf{u}^TP^L\mathbf{u}_t + a\mathbf{u}^TQ^L\mathbf{u} = &\varepsilon\mathbf{u}^TP^LD_2^L\mathbf{u} + \sigma_1^L\mathbf{u}^T\mathbf{e}_N^L(u_N - v_0) + \\ &\sigma_2^L\mathbf{u}^T\mathbf{e}_N^L\left[(D_{1B}^L\mathbf{u})_N - (D_{1B}^R\mathbf{v})_0\right] + \\ &\sigma_3^L(D_{1B}^L\mathbf{u})^T\mathbf{e}_N^L(u_N - v_0) + \mathbf{u}^T\mathrm{BT}^L,\end{aligned} \tag{11a}$$

$$\begin{aligned}\mathbf{v}^TP^R\mathbf{v}_t + a\mathbf{v}^TQ^R\mathbf{v} = &\varepsilon\mathbf{v}^TP^RD_2^R\mathbf{v} + \sigma_1^R\mathbf{v}^T\mathbf{e}_0^R(v_0 - u_N) + \\ &\sigma_2^R\mathbf{v}^T\mathbf{e}_0^R\left[(D_{1B}^R\mathbf{v})_0 - (D_{1B}^L\mathbf{u})_N\right] + \\ &\sigma_3^R(D_{1B}^R\mathbf{v})^T\mathbf{e}_0^R(v_0 - u_N) + \mathbf{v}^T\mathrm{BT}^R.\end{aligned} \tag{11b}$$

By adding the transposes and summing up we get

$$
\begin{aligned}
\frac{d}{dt}\left(\|\mathbf{u}\|^2_{P^L}+\|\mathbf{v}\|^2_{P^R}\right) = &-a\mathbf{u}^T\left[Q^L+(Q^L)^T\right]\mathbf{u}\\
&+\varepsilon\mathbf{u}^T\left[P^LD_2^L+(P^LD_2^L)^T\right]\mathbf{u}\\
&+2\sigma_1^L\mathbf{u}^T\mathbf{e}_N^L(u_N-v_0)\\
&+2\sigma_2^L\mathbf{u}^T\mathbf{e}_N^L\left[(D_{1B}^L\mathbf{u})_N-(D_{1B}^R\mathbf{v})_0\right]\\
&+2\sigma_3^L(D_{1B}^L\mathbf{u})^T\mathbf{e}_N^L(u_N-v_0)+2\mathbf{u}^T\mathrm{BT}^L\\
&-a\mathbf{v}^T\left[Q^R+(Q^R)^T\right]\mathbf{v}\\
&+\varepsilon\mathbf{u}^T\left[P^RD_2^R+(P^RD_2^R)^T\right]\mathbf{u}\\
&+2\sigma_1^R\mathbf{v}^T\mathbf{e}_0^R(v_0-u_N)\\
&+2\sigma_2^R\mathbf{v}^T\mathbf{e}_0^R\left[(D_{1B}^R\mathbf{v})_0-(D_{1B}^L\mathbf{u})_N\right]\\
&+2\sigma_3^R(D_{1B}^R\mathbf{v})^T\mathbf{e}_0^R(v_0-u_N)+2\mathbf{v}^T\mathrm{BT}^R.
\end{aligned}
\tag{12}
$$

Recall that

$$
\begin{aligned}
&\mathbf{u}^T\mathbf{e}_0^L=u_0, &&\mathbf{u}^T\mathbf{e}_N^L=u_N, &&\mathbf{u}^T[Q^L+(Q^L)^T]\mathbf{u}=u_N^2-u_0^2,\\
&\mathbf{v}^T\mathbf{e}_0^R=v_0, &&\mathbf{v}^T\mathbf{e}_N^R=v_N, &&\mathbf{v}^T[Q^R+(Q^R)^T]\mathbf{v}=v_N^2-v_0^2.
\end{aligned}
\tag{13}
$$

By using the relations in (6) and (13) Equation (12) reduces to

$$
\begin{aligned}
\frac{d}{dt}\left(\|\mathbf{u}\|^2_{P^L}+\|\mathbf{v}\|^2_{P^R}\right)&+2\varepsilon\mathrm{Diss}^L+2\varepsilon\mathrm{Diss}^R\\
&=au_0^2-au_N^2-2\varepsilon u_0(D_{1B}^L\mathbf{u})_0\\
&+2\varepsilon u_N(D_{1B}^L\mathbf{u})_N+2\sigma_1^Lu_N(u_N-v_0)\\
&+2\sigma_2^Lu_N\left[(D_{1B}^L\mathbf{u})_N-(D_{1B}^R\mathbf{v})_0\right]\\
&+2\sigma_3^L(D_{1B}^L\mathbf{u})_N(u_N-v_0)+2\mathbf{u}^T\mathrm{BT}^L\\
&+av_0^2-av_N^2-2\varepsilon v_0(D_{1B}^R\mathbf{v})_0\\
&+2\varepsilon v_N(D_{1B}^R\mathbf{v})_N+\sigma_1^Rv_0(v_0-u_N)\\
&+2\sigma_2^Rv_0\left[(D_{1B}^R\mathbf{v})_0-(D_{1B}^L\mathbf{u})_N\right]\\
&+2\sigma_3^R(D_{1B}^R\mathbf{v})_0(v_0-u_N)+2\mathbf{v}^T\mathrm{BT}^R,
\end{aligned}
\tag{14}
$$

where

$$
\mathrm{Diss}^L=\begin{cases}\|D_1\mathbf{u}\|^2_{P^L}, & \text{if } D_2^L=D_{2n}^L\\ (\mathbf{u},\mathbf{u})_{A^L+(A^L)^T}, & \text{if } D_2^L=D_{2c}^L\end{cases},
$$

and

$$
\mathrm{Diss}^R=\begin{cases}\|D_1\mathbf{u}\|^2_{P^R}, & \text{if } D_2^R=D_{2n}^R\\ (\mathbf{u},\mathbf{u})_{A^R+(A^R)^T}, & \text{if } D_2^R=D_{2c}^R\end{cases}.
$$

Equation (14) can be written in matrix form

$$\frac{d}{dt}\left(\|\mathbf{u}\|^2_{PL} + \|\mathbf{v}\|^2_{PR}\right) + 2\varepsilon \mathrm{Diss}^L + 2\varepsilon \mathrm{Diss}^R = \mathbf{u}_I^T M_I \mathbf{u}_I + \mathrm{BT}. \tag{15}$$

where BT collects all terms on the outer boundaries, that is,

$$\mathrm{BT} = 2\mathbf{u}\cdot \mathrm{BT}^L + au_0^2 - 2\varepsilon u_0 (D^L_{1B}\mathbf{u})_0 + 2\mathbf{v}\cdot \mathrm{BT}^R - av_N^2 + 2\varepsilon v_N (D^R_{1B}\mathbf{v})_N,$$

and

$$\mathbf{u}_I = \left[\begin{array}{cccc} u_N & (D^L_{1B}\mathbf{u})_N & v_0 & (D^R_{1B}\mathbf{v})_0 \end{array}\right]^T,$$

$$M_I = \begin{bmatrix} -a + 2\sigma_1^L & \varepsilon + \sigma_2^L + \sigma_3^L & -\sigma_1^L - \sigma_1^R & -\sigma_2^L - \sigma_3^R \\ \varepsilon + \sigma_2^L + \sigma_3^L & 0 & -\sigma_3^L - \sigma_2^R & 0 \\ -\sigma_1^L - \sigma_1^R & -\sigma_3^L - \sigma_2^R & a + 2\sigma_1^R & -\varepsilon + \sigma_2^R + \sigma_3^R \\ -\sigma_2^L - \sigma_3^R & 0 & -\varepsilon + \sigma_2^R + \sigma_3^R & 0 \end{bmatrix},$$

We need a negative semi-definite M_I for stability. Note that every sub-matrix in the matrix M_I should be negative semi-definite in order to ensure negative definiteness. Naturally the 2×2 sub-matrices along the diagonal should be negative semi-definite, which yields the necessary conditions,

$$-a + 2\sigma_1^L \leq 0, \qquad a + 2\sigma_1^R \leq 0, \tag{16}$$

and

$$\varepsilon + \sigma_2^L + \sigma_3^L = 0, \quad -\varepsilon + \sigma_2^R + \sigma_3^R = 0, \quad -\sigma_3^L - \sigma_2^R = 0. \tag{17}$$

The conditions (17) inserted into matrix M_I yields,

$$M_I = \begin{bmatrix} -a + 2\sigma_1^L & 0 & -\sigma_1^L - \sigma_1^R & 0 \\ 0 & 0 & 0 & 0 \\ -\sigma_1^L - \sigma_1^R & 0 & a + 2\sigma_1^R & 0 \\ 0 & 0 & 0 & 0 \end{bmatrix}.$$

We can verify that M_I is negative semi-definite if

$$\sigma_1^L \leq \frac{a}{2}, \qquad \sigma_1^R = \sigma_1^L - a, \tag{18}$$

which also satisfies (16).

The following proposition has been proved.

Proposition 3.2 *Consider the semi-discrete scheme (10) for the well-posed problem (1). If*

$$\begin{aligned} &\sigma_1^L \leq \frac{a}{2}, && \sigma_1^R = \sigma_1^L - a, && \\ &\sigma_2^R = \varepsilon + \sigma_2^L, && \sigma_3^L = -\varepsilon - \sigma_2^L, && \sigma_3^R = -\sigma_2^L. \end{aligned} \tag{19}$$

and Proposition 3.1 *holds, then (10) is stable.*

3.2.2 The "borrowing" method

In [3] the authors used $\sigma_3^L = \sigma_3^R = 0$ in the interface treatment. The semi-discrete approximation of (1) is given by

$$\begin{aligned}\mathbf{u}_t + aD_1^L\mathbf{u} =& \varepsilon D_2^L\mathbf{u} + \sigma_1^L(P^L)^{-1}\mathbf{e}_N^L(u_N - v_0) + \\ & \sigma_2^L(P^L)^{-1}\mathbf{e}_N^L\left[(D_{1B}^L\mathbf{u})_N - (D_{1B}^R\mathbf{v})_0\right] + \mathrm{BT}^L,\end{aligned} \tag{20a}$$

on the left subdomain, and

$$\begin{aligned}\mathbf{v}_t + aD_1^R\mathbf{v} =& \varepsilon D_2^R\mathbf{v} + \sigma_1^R(P^R)^{-1}\mathbf{e}_0^R(v_0 - u_N) + \\ & \sigma_2^R(P^R)^{-1}\mathbf{e}_0^R\left[(D_{1B}^R\mathbf{v})_0 - (D_{1B}^L\mathbf{u})_N\right] + \mathrm{BT}^R,\end{aligned} \tag{20b}$$

on the right subdomain. BT^L and BT^R represent the stable left and right boundary terms respectively.

Applying the energy method introduced in Section 3.2.1, we obtain the interface matrix M_I,

$$M_I = \begin{bmatrix} -a + 2\sigma_1^L & \varepsilon + \sigma_2^L & -\sigma_1^L - \sigma_1^R & -\sigma_2^L \\ \varepsilon + \sigma_2^L & 0 & -\sigma_2^R & 0 \\ -\sigma_1^L - \sigma_1^R & -\sigma_2^R & a + 2\sigma_1^R & -\varepsilon + \sigma_2^R \\ -\sigma_2^L & 0 & -\varepsilon + \sigma_2^R & 0 \end{bmatrix}.$$

The zero elements on the diagonal of M_I was filled in by "borrowing" portions from the terms Diss^L and Diss^R.

Note that the following relations hold

$$\begin{aligned}\mathrm{Diss}^L &= \kappa^L(D_{1B}^L\mathbf{u})_N^2 + \widehat{\mathrm{Diss}}^L, \\ \mathrm{Diss}^R &= \kappa^R(D_{1B}^R\mathbf{v})_0^2 + \widehat{\mathrm{Diss}}^R,\end{aligned}$$

where κ^L, $\kappa^R > 0$ and $\widehat{\mathrm{Diss}}^L$, $\widehat{\mathrm{Diss}}^R > 0$. Note that κ^L, κ^R are proportional to the mesh sizes in the left and right domain respectively.

With this substitution equation (15) becomes

$$\frac{d}{dt}\left(\|\mathbf{u}\|_{P^L}^2 + \|\mathbf{v}\|_{P^R}^2\right) + 2\varepsilon\widehat{\mathrm{Diss}}^L + 2\varepsilon\widehat{\mathrm{Diss}}^R = \mathbf{u}_I^T M_I' \mathbf{u}_I + \mathrm{BT} \tag{21}$$

with

$$M_I' = \begin{bmatrix} -a + 2\sigma_1^L & \varepsilon + \sigma_2^L & -\sigma_1^L - \sigma_1^R & -\sigma_2^L \\ \varepsilon + \sigma_2^L & -2\varepsilon\kappa^L & -\sigma_2^R & 0 \\ -\sigma_1^L - \sigma_1^R & -\sigma_2^R & a + 2\sigma_1^R & -\varepsilon + \sigma_2^R \\ -\sigma_2^L & 0 & -\varepsilon + \sigma_2^R & -2\varepsilon\kappa^R \end{bmatrix}.$$

and

$$\mathrm{BT} = 2\mathbf{u}\cdot \mathrm{BT}^L + au_0^2 - 2\varepsilon u_0(D_{1B}^L\mathbf{u})_0 + 2\mathbf{v}\cdot\mathrm{BT}^R - av_N^2 + 2\varepsilon v_N(D_{1B}^R\mathbf{v})_N.$$

A sufficient condition for semi-negative definiteness of M_I' derived in [3] is written,

$$\sigma_1^R = \sigma_1^L - a, \quad \sigma_2^R = \varepsilon + \sigma_2^L, \quad \sigma_1^L \le \frac{a}{2} - \frac{1}{4\varepsilon}\left[\frac{(\sigma_2^R)^2}{\kappa^L} + \frac{(\sigma_2^L)^2}{\kappa^R}\right]. \tag{22}$$

The following proposition was proved in [3].

Proposition 3.3 *Consider the semi-discrete scheme (20) for the well-posed problem (1). If the conditions in (22) and* Proposition 3.1 *are satisfied, then (20) is stable.*

A drawback with this interface treatment is that the coefficients depend on κ^L and κ^R, which in term depend on the mesh size. As a result, all coefficients must be modified, when the grid is refined.

3.2.3 The local discontinuous Galerkin method

By using the so called local discontinuous Galerkin (LDG) method (first introduced in [18], see also [4] and [19]), equation (1a) is written in first order form

$$\begin{aligned} u_t + au_x - \varepsilon p_x &= \sigma_1^L(u-v)\delta(x_i) + \sigma_2^L(p-q)\delta(x_i) \\ -\varepsilon u_x + \varepsilon p &= \sigma_3^L(u-v)\delta(x_i) \end{aligned} \qquad x\in[0,x_i], \tag{23a}$$

and

$$\begin{aligned} v_t + av_x - \varepsilon q &= \sigma_1^R(v-u)\delta(x_i) + \sigma_2^R(q-p)\delta(x_i) \\ -\varepsilon v_x + \varepsilon q &= \sigma_3^R(v-u)\delta(x_i) \end{aligned} \qquad x\in[x_i,1]. \tag{23b}$$

In (23) x_i denotes the location of the interface and $p\approx u_x$ and $q\approx v_x$ are intermediate variables. $\delta(x_i)$ is the delta function.

For $u,p\in V_{(0,x_i)}$ in (23a) there exist two test functions $\phi^L,\psi^L\in V_{(0,x_i)}$ such that

$$\begin{aligned} &\int_0^{x_i}\phi^L u_t\,dx + a\int_0^{x_i}\phi^L u_x\,dx - \varepsilon\int_0^{x_i}\phi^L p_x\,dx \\ &\quad = \sigma_1^L\int_0^{x_i}\phi^L(u-v)\delta(x_i)\,dx + \sigma_2^L\int_0^{x_i}\phi^L(p-q)\delta(x_i)\,dx \end{aligned} \tag{24a}$$

and

$$-\varepsilon\int_0^{x_i}\psi^L u_x\,dx + \varepsilon\int_0^{x_i}\psi^L p\,dx = \sigma_3^L\int_0^{x_i}\psi^L(u-v)\delta(x_i)\,dx. \tag{24b}$$

By using the integration by parts, we have

$$
\begin{aligned}
\int_0^{x_i} \phi^L u_t\,dx - a\int_0^{x_i} \phi^L_x u\,dx + \varepsilon\int_0^{x_i} \phi^L_x p\,dx - a\phi^L(0)u(0) + \varepsilon\phi^L(0)p(0)& \\
= - a\phi^L(x_i)u(x_i) + \varepsilon\phi^L(x_i)p(x_i)& \\
+ \sigma^L_1\phi^L(x_i)\big[u(x_i) - v(x_i)\big] + \sigma^L_2\phi^L(x_i)\big[p(x_i) - q(x_i)\big]& \\
= - a\phi^L(x_i)\Big[\big(1 - \frac{\sigma^L_1}{a}\big)u(x_i) + \frac{\sigma^L_1}{a}v(x_i)\Big]& \\
+ \varepsilon\phi^L(x_i)\Big[\big(1 + \frac{\sigma^L_2}{\varepsilon}\big)p(x_i) - \frac{\sigma^L_2}{\varepsilon}q(x_i)\Big]& \\
= - a\phi^L(x_i)\bar{u}^L_{x_i}(x_i) + \varepsilon\phi^L(x_i)\bar{p}^L_V(x_i),&
\end{aligned} \tag{25a}
$$

and

$$
\begin{aligned}
-\varepsilon\int_0^{x_i} \psi^L_x u\,dx + \varepsilon\int_0^{x_i} \psi^L p\,dx + \varepsilon\psi^L(0)u(0)& \\
=\varepsilon\psi^L(x_i)u(x_i) + \sigma^L_3\psi^L(x_i)\big[u(x_i) - v(x_i)\big]& \\
=\varepsilon\psi^L(x_i)\Big[\big(1 + \frac{\sigma^L_3}{\varepsilon}\big)u(x_i) - \frac{\sigma^L_3}{\varepsilon}v(x_i)\Big]& \\
=\varepsilon\psi^L(x_i)\bar{u}^L_V(x_i),&
\end{aligned} \tag{25b}
$$

where we have introduced the modified fluxes $\bar{u}^L_{x_i}(x_i)$, $\bar{u}^L_V(x_i)$ and $\bar{p}^L_V(x_i)$. They are

$$
\begin{aligned}
\bar{u}^L_{x_i}(x_i) &= \big(1 - \frac{\sigma^L_1}{a}\big)u(x_i) + \frac{\sigma^L_1}{a}v(x_i), \\
\bar{p}^L_V(x_i) &= \big(1 + \frac{\sigma^L_2}{\varepsilon}\big)p(x_i) - \frac{\sigma^L_2}{\varepsilon}q(x_i), \\
\bar{u}^L_V(x_i) &= \big(1 + \frac{\sigma^L_3}{\varepsilon}\big)u(x_i) - \frac{\sigma^L_3}{\varepsilon}v(x_i),
\end{aligned} \tag{26}
$$

respectively.

Similarly, for $v, q \in V_{(x_i,1)}$ in (23b) there exist two test functions $\phi^R, \psi^R \in V_{(0,x_i)}$ such that

$$
\begin{aligned}
\int_{x_i}^1 \phi^R v_t\,dx - a\int_{x_i}^1 \phi^R_x v\,dx + \varepsilon\int_{x_i}^1 \phi^R_x q\,dx + a\phi^R(1)u(1) - \varepsilon\phi^R(1)p(1)& \\
= a\phi^R(x_i)\bar{u}^R_{x_i}(x_i) - \varepsilon\phi^R(x_i)\bar{p}^R_V(x_i),&
\end{aligned} \tag{27a}
$$

$$
\varepsilon\int_{x_i}^1 \psi^R_x u\,dx + \varepsilon\int_{x_i}^1 \psi^R p\,dx - \varepsilon\psi^R(1)u(1) = -\varepsilon\psi^R(x_i)\bar{u}^R_V(x_i), \tag{27b}
$$

where the modified fluxed $\bar{u}^R_{x_i}(x_i)$, $\bar{p}^R_V(x_i)$, and $\bar{u}^R_V(x_i)$ are

$$
\begin{aligned}
\bar{u}^R_{x_i}(x_i) &= \big(1+\frac{\sigma_1^R}{a}\big)u(x_i) - \frac{\sigma_1^R}{a}v(x_i),\\
\bar{p}^R_V(x_i) &= \big(1-\frac{\sigma_2^R}{\varepsilon}\big)p(x_i) + \frac{\sigma_2^R}{\varepsilon}q(x_i),\\
\bar{u}^R_V(x_i) &= \big(1-\frac{\sigma_3^R}{\varepsilon}\big)u(x_i) + \frac{\sigma_3^R}{\varepsilon}v(x_i),
\end{aligned}
\tag{28}
$$

respectively.

Different types of fluxes can be obtained via a choice of the coefficients $\sigma_1^L(x_i)$, $\sigma_1^R(x_i)$, $\sigma_2^L(x_i)$, $\sigma_2^R(x_i)$, $\sigma_3^L(x_i)$ and $\sigma_3^R(x_i)$ in (26) and (28). The following centered fluxes and the one-sided fluxes are suggested in [19]. With the choice

$$
\begin{aligned}
\sigma_1^L &= \frac{a}{2}, & \sigma_1^R &= -\frac{a}{2},\\
\sigma_2^L &= -\frac{\varepsilon}{2}, & \sigma_2^R &= \frac{\varepsilon}{2},\\
\sigma_3^L &= -\frac{\varepsilon}{2}, & \sigma_3^R &= \frac{\varepsilon}{2},
\end{aligned}
\tag{29}
$$

the centered fluxes becomes,

$$
\begin{aligned}
\bar{u}^L_{x_i}(x_i) = \bar{u}^R_{x_i}(x_i) = \bar{u}^L_V(x_i) = \bar{u}^R_V(x_i) &= \frac{1}{2}\big(u(x_i)+v(x_i)\big),\\
\bar{p}^L_V = \bar{p}^R_V &= \frac{1}{2}\big(p(x_i)+q(x_i)\big).
\end{aligned}
\tag{30}
$$

Moreover, when

$$
\begin{aligned}
\sigma_1^L &= 0, & \sigma_1^R &= -a,\\
\sigma_2^L &= -\varepsilon, & \sigma_2^R &= 0,\\
\sigma_3^L &= 0, & \sigma_3^R &= \varepsilon,
\end{aligned}
\tag{31}
$$

the one-sided fluxes are given by

$$
\begin{aligned}
\bar{u}^L_{x_i}(x_i) &= u(x_i), & \bar{u}^R_{x_i}(x_i) &= v(x_i),\\
\bar{p}^L_V(x_i) &= q(x_i), & \bar{p}^R_V(x_i) &= p(x_i),\\
\bar{u}^L_V(x_i) &= u(x_i), & \bar{u}^R_V(x_i) &= v(x_i).
\end{aligned}
\tag{32}
$$

Now we consider the semi-discrete approximation of (23). A semi-discrete scheme is written by

$$
\begin{aligned}
\mathbf{u}_t + aD_1^L\mathbf{u} - \varepsilon D_1^L\mathbf{p} =& \sigma_1^L(P^L)^{-1}\mathbf{e}_N^L(u_N - v_0) + \\
& \sigma_2^L(P^L)^{-1}\mathbf{e}_N^L(p_N - q_0) + \mathrm{BT}^L\\
-\varepsilon D_1^L\mathbf{u} + \varepsilon\mathbf{p} =& \sigma_3^L(P^L)^{-1}\mathbf{e}_N^L(u_N - v_0)
\end{aligned}
\tag{33a}
$$

on the left subdomain, and

$$\begin{aligned} \mathbf{v}_t + aD_1^R\mathbf{v} - \varepsilon D_1^R\mathbf{q} =& \sigma_1^R(P^R)^{-1}\mathbf{e}_0^R(v_0 - u_N) + \\ & \sigma_2^R(P^R)^{-1}\mathbf{e}_0^R(q_0 - p_N) + \mathrm{BT}^R \\ -\varepsilon D_1^R\mathbf{v} + \varepsilon\mathbf{q} =& \sigma_3^R(P^R)^{-1}\mathbf{e}_0^R(v_0 - u_N) \end{aligned} \tag{33b}$$

on the right subdomain. In (33) we have $p \approx D_1^L\mathbf{u}$ and $q \approx D_1^R\mathbf{v}$.

Proposition 3.4 *The conditions (19) in Proposition 3.2 lead to stability the LDG method.*

Proof: Applying the energy method introduced in Section 3.2.1 to (33) yields

$$\frac{d}{dt}\left(\|\mathbf{u}\|_{P^L}^2 + \|\mathbf{v}\|_{P^R}^2\right) + 2\varepsilon\|\mathbf{p}\|_{P^L}^2 + 2\varepsilon\|\mathbf{q}\|_{P^R}^2 = \mathbf{v}_I^T M_I \mathbf{v}_I + \mathrm{BT}, \tag{34}$$

where M_I and BT are given in (15) and $\mathbf{v}_I = [u_N \quad p_N \quad v_0 \quad q_0]^T$.

Consequently, the conditions (19) also lead to an energy estimate for the LDG method. ■

Remark: Since the relations in (29) and (31) for centered and one-sided fluxes are subsets of (19), the LDG scheme (33) with the centered or one-sided fluxes has an energy estimate.

4 Eigenvalue analysis

We will compare the eigenvalue of the semi-discrete problem with the corresponding continuous eigenvalues.

4.1 The spectrum of the continuous problem

The Laplace transform of (1) with zero initial data gives

$$\begin{aligned} & s\tilde{u} + a\tilde{u}_x = \varepsilon\tilde{u}_{xx}, \qquad 0 \leq x \leq 1 \\ & \tilde{u}(0) + \beta\tilde{u}_x = 0, \quad \tilde{u}_x(1) = 0. \end{aligned} \tag{35}$$

where we have chosen $\alpha = 1$, $\gamma = 0$ and $\delta = 1$ as an example.

The general solution of (35) is

$$\tilde{u} = \sigma_1 e^{\kappa_1 x} + \sigma_2 e^{\kappa_2 x},$$

with

$$\kappa_{1,2} = \frac{a}{2\varepsilon}\left(1 \pm \sqrt{1 + \frac{4\varepsilon}{a^2}s}\right).$$

By applying the boundary conditions and demanding a unique solution we obtain that the Kreiss condition (see [7]) for stability of (35) is

$$\det C(s) = \begin{vmatrix} 1+\beta\kappa_1 & 1+\beta\kappa_2 \\ \kappa_1 e^{\kappa_1} & \kappa_2 e^{\kappa_2} \end{vmatrix} \neq 0 \quad \text{for } \Re(s) \geq 0.$$

The spectrum of the continuous problem consist of s-values making

$$\det C(s) = (1+\beta\kappa_2)\kappa_1 e^{\kappa_1} - (1+\beta\kappa_1)\kappa_2 e^{\kappa_2} = 0, \tag{36}$$

(for more details, see [9]).

We have the following lemma.

Lemma 4.1 *Equation (36) has a solution if $s \leq -a^2/(4\varepsilon)$, $s \in \Re$.*

The proof is presented in Appendix.

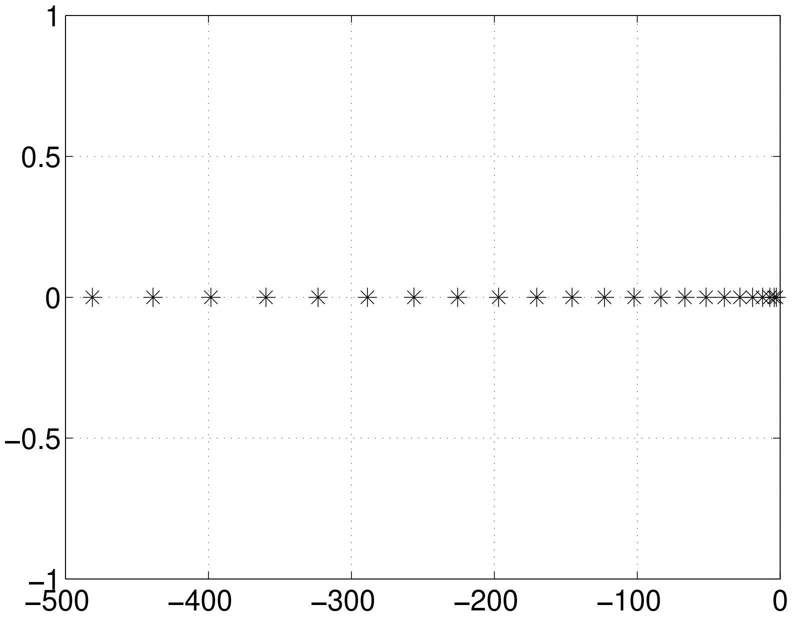

Figure 1: The part of spectrum for the continuous system. $\max(\Re(\lambda_i)) = -2.67261695452793$.

By choosing $a = 1$, $\varepsilon = 0.1$ and $\beta = -2\varepsilon/a = -0.2$ in (35), we obtain the two maximum eigenvalues $s_c^1 = -2.67261695452793$ and $s_c^2 = -4.12696691192682$ for the continuous system in (35). The least negative part of the spectrum for continuous system is presented in Figure 1. Note that the eigenvalues are real.

4.2 The spectrum of the semi-discrete problem

It is convenient to introduce notations for the methods introduced in the previous sections. If the approximation for the second derivative SBP operator is of the form $D_2 = D_1 \cdot D_1$ we denote it the *non-compact* form. The formulation $D_2 = P^{-1}(-A + BS)$ is denoted the *compact* form. Moreover, we denote

SIN: the scheme (5b) with non-compact form on single domain;

SIC: the scheme (5b) with compact form on single domain;

BAN: the Baumann-Oden scheme (10) with non-compact form;

BAC: the Baumann-Oden scheme(10) with compact form;

BON: the borrowing scheme (20) with non-compact form;

BOC: the borrowing scheme (20) with compact form;

LDG: the local discontinuous Galerkin method (33) (No compact form);

CON: the continuous system (1).

All the semi-discrete schemes can be written in the form,

$$\mathbf{u}_t = A\mathbf{u} + \tilde{F},$$

where A is a matrix and $\tilde{F}$ is a function of F, g^L and g^R given in (1). Note that the matrix A may not be symmetric since we introduce boundary and interface terms. This means that some parts of the spectra can be complex. If the number of grid points $N \to \infty$ the spectra of the semi-discrete problems should converge to the spectra of the continuous problems since our approximations are stable and accurate. For a finite number of grid points, part of the spectra of semi-discrete problem corresponds to the spectra of the continuous problem.

We compare the spectra of these schemes in the two subdomains with uniform mesh of 160 grid points. The computation on $[0, 1]$ is divided into two subdomains $[0, 1/2]$ and $[1/2, 1]$. For the BAN, BAC, and LDG schemes, we choose the coefficients $\sigma_1^L = a/2 = 1/2$ and $\sigma_2^L = \varepsilon$. The other coefficients can be decided by the stability conditions in (19). In the BON and BOC schemes, the coefficient σ_1^L depends on κ^L and κ^R, which increase with grid refinement. In all tests, σ_1^L, is determined by the maximum value under the stability condition (22), that is,

$$\sigma_1^L = \frac{a}{2} - \frac{1}{4\varepsilon}\left[\frac{(\sigma_2^R)^2}{\kappa^L} + \frac{(\sigma_2^L)^2}{\kappa^R}\right].$$

Table 1 presents that the maximum eigenvalues for different ε ($a = 1$). Note that LDG cannot employ the compact form to discretize the second derivative. Due to the compact form, the maximum eigenvalues of SIC, BAC, and BOC agree well with the continuous system (see Table 1). But for the non-compact form, if ε is small ($\varepsilon \leq 0.06$ for the second order as well as $\varepsilon \leq 0.04$ for the sixth order), the maximum eigenvalues of the semi-discrete schemes do not correspond to that of the continuous system.

Denote the convergence rate q_e for the maximum eigenvalue by

$$q_e = \frac{\log_{10}\left(|s_c - s_d^{(1)}|/|s_c - s_d^{(2)}|\right)}{\log_{10}\left(N^{(1)}/N^{(2)}\right)} \tag{37}$$

where s_c and s_d are the maximum eigenvalues of the continuous system and semi-discrete schemes. $s_d^{(1)}$ and $s_d^{(2)}$ are the maximum eigenvalues on the meshes of $N^{(1)}$ and $N^{(2)}$ grid points (including boundary points), respectively. The convergence rate q_e with $a = 1$ and $\varepsilon = 0.1$ are shown in Tables 2 and 3. The eigenvalues of the semi-discrete system converges to the eigenvalues of continuous system with the grid refinement. With non-compact form, the SIN and LDG schemes have higher precision. For example, by using the sixth order accuracy SBP operator and 80 grid points, the SIN has eight digits precision while both BAN and BON have 6 digits precision on multiple domain. The convergence rates of the non-compact forms (SIN, BAN and BON) are almost similar to those of the compact forms (SIC, BAC and BOC). However there are significant differences in error levels between the non-compact form and compact form (see Tables 2 and 3).

To speed up convergence to steady state and increase computational efficiency it is essential that the spectral radius of the numerical scheme is minimal. In (19) there are six unknown variables and four equations. Let σ_1^L and σ_2^L be the free parameters.
Table 4 shows the spectral radius of these schemes on a uniform mesh of 161 grid points on two subdomains with different σ_2^L. σ_1^L is fixed to $a/2$. We do not present more results with different σ_1^L since σ_1^L only affect the results marginally when $\sigma_l^L \in [-a, a/2]$. The spectral radius are almost same for all these schemes if reasonable coefficients are chosen. From these tables we find that $\sigma_2^L = \mathcal{O}(\varepsilon)$ minimize the spectrum radius. We note that the LDG scheme always has a minimal spectral radius when $\sigma_1^L = a/2$ and $\sigma_2^L = -\varepsilon/2$, that is, with the centered fluxes. When $\sigma_1^L = 0$ and $\sigma_2^L = -\varepsilon$ the one-sided fluxes (see [19]) have been obtained. In this case, the LDG scheme has a rather small spectral radius (see Table 4).

Remark All the semi-discrete approximations of (1) have spectra located in the left half of the complex plane, which means that the long-time behavior

(a) Second order accuracy

ε	0.005	0.01	0.02	0.05	0.1	0.2
SIN	−3.3187	−3.9873	−4.6158	−4.6724	−2.6732	−1.5110
BAN	−3.8587	−4.8050	−5.6747	−5.0748	−2.6732	−1.5110
BON	−3.9489	−5.4306	−6.7694	−5.1153	−2.6732	−1.5110
LDG	−3.4369	−4.0825	−4.7007	−4.7111	−2.6728	−1.5110
SIC	−28.8214	−23.5382	−12.6223	−5.1068	−2.6732	−1.5110
BAC	−29.6753	−22.5115	−12.6223	−5.1068	−2.6732	−1.5110
BOC	−29.6825	−22.5296	−12.6223	−5.1068	−2.6732	−1.5110
CON	−49.3632	−25.2135	−12.4380	−5.1021	−2.6726	−1.5109

(b) Fourth order accuracy

ε	0.005	0.01	0.02	0.05	0.1	0.2
SIN	−4.6742	−5.7632	−6.7863	−5.1038	−2.6726	−1.5109
BAN	−5.4991	−6.9403	−8.1308	−5.1022	−2.6726	−1.5109
BON	−6.0137	−8.2626	−9.7853	−5.1024	−2.6726	−1.5109
LDG	−4.7927	−5.8636	−6.8652	−5.1035	−2.6726	−1.5109
SIC	−29.6059	−23.2196	−12.5452	−5.1021	−2.6726	−1.5109
BAC	−30.1122	−22.9474	−12.5452	−5.1021	−2.6726	−1.5109
BOC	−30.1123	−22.6945	−12.5452	−5.1021	−2.6726	−1.5109
CON	−49.3632	−25.2135	−12.4380	−5.1021	−2.6726	−1.5109

(c) Sixth order accuracy

ε	0.005	0.01	0.02	0.05	0.1	0.2
SIN	−5.1959	−6.4197	−7.7066	−5.1021	−2.6726	−1.5109
BAN	−6.1718	−7.7586	−9.1441	−5.1021	−2.6726	−1.5109
BON	−6.7816	−9.2849	−10.8014	−5.1021	−2.6726	−1.5109
LDG	−5.3114	−6.5127	−8.3412	−5.1021	−2.6726	−1.5109
SIC	−29.3339	−22.9183	−12.5456	−5.1021	−2.6726	−1.5109
BAC	−28.9662	−22.5006	−12.5456	−5.1021	−2.6726	−1.5109
BOC	−27.9956	−23.7056	−12.5456	−5.1021	−2.6726	−1.5109
CON	−49.3632	−25.2135	−12.4380	−5.1021	−2.6726	−1.5109

Table 1: The maximum eigenvalues with 160 grid points. $a = 1$.

(a) Second order accuracy

Points	SIN		BAN		BON		LDG	
	$\lvert s_d - s_c \rvert$	q_e	$\lvert s_d - s_c \rvert$	q_e	$\lvert s_d - s_c \rvert$	q_e	$\lvert s_d - s_c \rvert$	q_e
40	$2.2e-02$		$3.3e-03$		$5.4e-03$		$1.8e-02$	
80	$1.8e-03$	3.69	$7.2e-04$	2.23	$9.2e-04$	2.58	$1.5e-03$	4.30
120	$4.9e-04$	3.26	$3.0e-04$	2.19	$3.5e-04$	2.35	$4.4e-04$	3.64
160	$2.1e-04$	2.86	$1.6e-04$	2.16	$1.8e-04$	2.29	$2.0e-04$	2.74
200	$1.2e-04$	2.62	$1.0e-04$	2.13	$1.1e-04$	2.24	$1.1e-04$	2.53

(b) Fourth order accuracy

Points	SIN		BAN		BON		LDG	
	$\lvert s_d - s_c \rvert$	q_e	$\lvert s_d - s_c \rvert$	q_e	$\lvert s_d - s_c \rvert$	q_e	$\lvert s_d - s_c \rvert$	q_e
40	$8.4e-05$		$1.3e-04$		$2.8e-04$		$7.1e-05$	
80	$1.0e-06$	6.46	$8.5e-06$	3.99	$1.8e-05$	4.02	$7.4e-07$	6.05
120	$7.7e-08$	6.41	$1.7e-06$	4.00	$3.6e-06$	4.01	$8.9e-08$	5.20
160	$1.2e-08$	6.38	$5.5e-07$	4.00	$1.1e-06$	4.01	$1.8e-08$	5.57
200	$5.5e-09$	3.68	$2.3e-07$	4.00	$4.7e-07$	4.00	$8.7e-09$	3.30

(c) Sixth order accuracy

Points	SIN		BAN		BON		LDG	
	$\lvert s_d - s_c \rvert$	q_e	$\lvert s_d - s_c \rvert$	q_e	$\lvert s_d - s_c \rvert$	q_e	$\lvert s_d - s_c \rvert$	q_e
40	$1.1e-05$		$6.5e-05$		$1.3e-04$		$9.9e-06$	
80	$6.4e-08$	7.38	$2.5e-06$	4.85	$5.0e-06$	4.79	$5.5e-08$	7.83
120	$2.9e-09$	7.60	$3.5e-07$	4.79	$7.0e-07$	4.80	$2.4e-09$	7.63
160	$3.1e-10$	7.81	$8.6e-08$	4.91	$1.7e-07$	4.92	$2.6e-10$	7.85
200	$5.3e-11$	7.88	$2.9e-08$	4.93	$5.8e-08$	4.93	$4.7e-11$	7.71

Table 2: The convergence rate of the maximum eigenvalue for non-compact form $D_2 = D_1 \cdot D_1$. s_d and s_c are the maximum eigenvalues for the semi-discrete schemes and continuous problem, respectively. $a = 1$ and $\varepsilon = 0.1$.

(a) Second order accuracy

Points	SIC		BAC		BOC	
	$\lvert s_d - s_c\rvert$	q_e	$\lvert s_d - s_c\rvert$	q_e	$\lvert s_d - s_c\rvert$	q_e
40	$8.9e-03$		$8.9e-03$		$8.8e-03$	
80	$2.2e-03$	2.05	$2.2e-03$	2.05	$2.2e-03$	2.05
120	$9.8e-04$	2.02	$9.8e-04$	2.01	$9.8e-04$	2.01
160	$5.5e-04$	2.01	$5.5e-04$	2.01	$5.5e-04$	2.00
200	$3.5e-04$	2.00	$3.5e-04$	2.00	$3.5e-04$	2.00

(b) Fourth order accuracy

Points	SIC		BAC		BOC	
	$\lvert s_d - s_c\rvert$	q_e	$\lvert s_d - s_c\rvert$	q_e	$\lvert s_d - s_c\rvert$	q_e
40	$1.9e-05$		$2.9e-05$		$4.5e-05$	
80	$1.2e-06$	4.13	$1.7e-06$	4.15	$2.7e-05$	4.16
120	$2.2e-07$	4.07	$3.3e-07$	4.09	$5.2e-07$	4.09
160	$7.1e-08$	4.05	$1.0e-07$	4.06	$1.6e-07$	4.06
200	$2.9e-08$	4.03	$4.2e-08$	4.05	$6.6e-08$	4.05

(c) Sixth order accuracy

Points	SIC		BAC		BOC	
	$\lvert s_d - s_c\rvert$	q_e	$\lvert s_d - s_c\rvert$	q_e	$\lvert s_d - s_c\rvert$	q_e
40	$1.7e-08$		$5.9e-08$		$2.2e-07$	
80	$1.5e-10$	6.99	$4.6e-09$	3.74	$1.6e-08$	3.89
120	$9.8e-12$	6.74	$8.8e-10$	4.09	$3.0e-09$	4.11
160	$7.1e-13$	9.23	$2.5e-10$	4.47	$8.4e-10$	4.51
200	$6.9e-12$	–	$8.0e-11$	5.09	$2.9e-10$	4.75

Table 3: The convergence rate of the maximum eigenvalue for compact form $D_2 = P^{-1}(-A + BS)$. s_d and s_c are the maximum eigenvalues for the semi-discrete schemes and continuous problem, respectively. $a = 1$ and $\varepsilon = 0.1$.

(a) Second order accuracy

σ_2^L	-10ε	$-\varepsilon$	$-\varepsilon/2$	0	$\varepsilon/2$	ε	10ε
BAN	$1.1e+5$	$7.1e+3$	$5.2e+3$	$6.6e+3$	$1.3e+4$	$2.0e+4$	$1.2e+5$
BON	$9.4e+5$	$5.2e+3$	$5.2e+3$	$5.6e+3$	$1.3e+4$	$2.5e+4$	$1.0e+6$
LDG	$3.7e+6$	$1.6e+4$	$5.2e+3$	$1.8e+4$	$4.7e+4$	$9.9e+4$	$4.5e+5$
BAC	$2.0e+5$	$1.2e+4$	$1.0e+4$	$1.2e+4$	$2.2e+4$	$3.3e+4$	$2.4e+5$
BOC	$9.4e+5$	$1.0e+4$	$1.0e+4$	$1.0e+4$	$1.3+4$	$2.3e+4$	$1.1e+6$

(b) Fourth order accuracy

σ_2^L	-10ε	$-\varepsilon$	$-\varepsilon/2$	0	$\varepsilon/2$	ε	10ε
BAN	$2.3e+5$	$1.3e+4$	$9.7e+3$	$1.2e+4$	$2.4e+4$	$3.6e+4$	$2.6e+5$
BON	$1.8e+6$	$9.9e+3$	$9.8e+3$	$9.9e+3$	$2.3e+4$	$4.7e+4$	$2.4e+6$
LDG	$7.2e+6$	$3.3e+4$	$9.7e+3$	$3.3e+4$	$9.5e+4$	$1.9e+5$	$8.9e+6$
BAC	$3.6e+5$	$2.3e+4$	$1.4e+4$	$2.2e+4$	$4.0e+4$	$5.8e+4$	$4.0e+5$
BOC	$1.8e+6$	$1.4e+4$	$1.4e+4$	$1.4e+4$	$1.8e+4$	$4.5e+4$	$2.3e+6$

(c) Sixth order accuracy

σ_2^L	-10ε	$-\varepsilon$	$-\varepsilon/2$	0	$\varepsilon/2$	ε	10ε
BAN	$3.1e+5$	$1.7e+4$	$1.6e+4$	$1.6e+4$	$3.1e+4$	$4.8e+4$	$3.3e+5$
BON	$2.4e+6$	$1.6e+4$	$1.5e+4$	$1.4e+4$	$3.0e+4$	$6.0e+4$	$2.9e+6$
LDG	$9.3e+6$	$4.4e+4$	$1.5e+4$	$4.4e+4$	$1.1e+5$	$2.4e+5$	$1.0e+7$
BAC	$5.6e+5$	$3.4e+4$	$3.4e+4$	$3.7e+4$	$3.7e+4$	$6.1e+4$	$6.1e+5$
BOC	$2.3e+6$	$3.6e+4$	$3.4e+4$	$3.6e+4$	$3.6e+4$	$5.3e+4$	$2.8e+6$

Table 4: The spectral radius. $a = 1$, $\varepsilon = 0.1$ and $\sigma_1^L = a/2$.

of the solution is correct.

5 Numerical experiments

Denote the convergence rate q in the computational domain by

$$q = \frac{\log_{10}\left(||u - v^{(1)}||_2/||u - v^{(2)}||_2\right)}{\log_{10}\left(N^{(1)}/N^{(2)}\right)} \tag{38}$$

where u is an exact solution. $v^{(1)}$ and $v^{(2)}$ are the corresponding numerical solutions on the meshes of $N^{(1)}$ and $N^{(2)}$ grid points (including boundary points), respectively.

With a diagonal norm, the first derivative SBP operator was constructed with $2p$-th order accuracy internal accuracy and p-th order at the boundary (see [8], [11] and [20]). According to [5], $(p+1)$-th order accuracy is achieved in a hyperbolic equation which only includes the first derivative. For example, an SBP operator with sixth order internal accuracy and third order accurate boundary closures will lead to a fourth order accurate scheme.

	2nd*+1st**	4th*+2nd**	6th*+3rd**
q with non-compact form	2	3	4
q with compact form	2	4	5

Table 5: The theoretical convergence rate by using different SBP operators with diagonal norm. * and ** represent the interior and the boundary accuracy of the first derivative, respectively.

In the advection-diffusion equation, as described previously, there are two options to construct the SBP operator for the second derivative. The non-compact form is obtained by using the first derivative operator $D_1 = P^{-1}Q$ twice, that is, $D_2 = D_1 \cdot D_1$. With a diagonal norm, we obtain a boundary closure of order $(p-1)$-th. In the compact form we use the minimal width operator $D_2 = P^{-1}(-A + BS)$, and the second derivative SBP operators have p-th order accuracy at the boundaries, see [11] for details. It was proved in [23] that if the solution is pointwise bounded, the accuracy of advection-diffusion equation is two orders higher than the accuracy of the second derivative approximation at the boundaries. For clarity, the theoretical convergence rate is shown in Table 5.

One exact solution to the advection-diffusion equation (1) is

$$u = \sin(w(x-ct))e^{-bx}, \qquad c > 0, \quad w = \frac{\sqrt{c^2 - a^2}}{2\varepsilon}, \quad b = \frac{c-a}{2\varepsilon}, \quad |c| > |a|.$$

In the following analysis we have chosen $a = 1$, $\varepsilon = 0.01$, $c = 1.01$ and $\alpha = 1$, $\beta = -0.01$, $\gamma = 0$, $\delta = 1$. We use the classical fourth-order Runge-Kutta method for the time integration. A small time-step is used to minimize the temporal errors.

5.1 Single domain

We begin by studying the accuracy of the SBP operators on a single domain. The convergence rate for both options of the second derivatives are shown in Table 6. The results are in line with the theoretical prediction in Table 5.

(a) non-compact form $D_2 = D_1 \cdot D_1$

	2nd order		4th order		6th order	
Points	L_2-Err	q	L_2-Err	q	L_2-Err	q
41	−1.10		−2.41		−2.38	
81	−1.71	2.05	−3.37	3.26	−3.55	3.95
161	−2.31	2.02	−4.29	3.08	−4.75	3.95
321	−2.91	2.00	−5.20	3.03	−5.94	4.02
641	−3.51	2.00	−6.11	3.01	−7.15	3.99

(b) compact form $D_2 = P^{-1}(-A + BS)$

	2nd order		4th order		6th order	
Points	L_2-Err	q	L_2-Err	q	L_2-Err	q
41	−1.11		−2.61		−3.0210	
81	−1.71	2.05	−3.85	4.21	−4.29	4.28
161	−2.32	2.02	−5.08	4.10	−5.82	5.14
321	−2.92	2.01	−6.29	4.04	−7.43	5.35
641	−3.52	2.01	−7.50	4.04	−9.06	5.35

Table 6: Grid convergence rate of approximation of $u_t + u_x = 0.01u_{xx}$ in a single domain $[-1, 1]$.

5.2 Two subdomains with an interface

Recall that the *LDG* method prohibits the use of the compact form for the second derivative. We apply the non-compact form for a fair comparison between the different methods. The convergence rates are calculated on two subdomains of uniform mesh with an interface at $x = 0$ (see Table 7). The uniform mesh is refined from 42 to 1282 grid points. As in the single domain case, the convergence rates for the non-compact formulation agree with the theory in [5], [6], [10], and [23]. Note that the convergence rate q_e of maximum eigenvalue with the non-compact form (see Table 2) is one order higher than the convergence rate q for the approximations (see Table 7).

(a) second order accuracy

	BAN		BON		LDG	
Points	L_2-Err	q	L_2-Err	q	L_2-Err	q
41	−1.07		−1.07		−1.07	
81	−1.69	2.13	−1.69	2.13	−1.70	2.14
161	−2.30	2.06	−2.30	2.06	−2.30	2.06
321	−2.90	2.02	−2.90	2.03	−2.91	2.03
641	−3.51	2.01	−3.51	2.01	−3.51	2.01

(b) fourth order accuracy

	BAN		BON		LDG	
Points	L_2-Err	q	L_2-Err	q	L_2-Err	q
41	−2.14		−2.00		−2.04	
81	−3.22	3.62	−3.97	3.28	−2.94	3.03
161	−4.14	3.08	−4.03	3.54	−4.5746	3.04
321	−5.01	2.91	−4.97	3.13	−5.7974	3.02
641	−5.89	2.95	−5.88	3.02	−6.9995	3.01

(c) sixth order accuracy

	BAN		BON		LDG	
Points	L_2-Err	q	L_2-Err	q	L_2-Err	q
41	−2.02		−2.02		−1.93	
81	−3.26	4.25	−3.28	4.40	−3.24	4.49
161	−4.55	4.37	−4.57	4.35	−4.62	4.67
321	−5.79	4.15	−5.80	4.09	−5.93	4.39
641	−7.00	4.00	−7.00	4.00	−7.17	4.14

Table 7: Grid convergence of approximations of $u_t + u_x = 0.01u_{xx}$ on two subdomains of uniform mesh in $[-1, 1]$.

Now the convergence rate q is tested on two subdomains with non-uniform grid. We start with 41 grid points in the left subdomain and 11 grid points in the right subdomain. For each refinement the grid points are doubled in both subdomains. Table 8 presents the results using a non-compact second derivative. The convergence rate exactly coincide with the theoretical values.

(a) second order accuracy

	BAN		BON		LDG	
Points	L_2-Err	q	L_2-Err	q	L_2-Err	q
$41+11$	-0.99		-0.93		-0.96	
$81+21$	-1.64	2.19	-1.63	2.29	-1.60	2.14
$161+41$	-2.26	2.12	-2.27	2.13	-2.22	2.05
$321+81$	-2.88	2.05	-2.89	2.03	-2.83	2.01
$641+161$	-3.48	2.01	-3.48	2.01	-3.43	2.00

(b) fourth order accuracy

	BAN		BON		LDG	
Points	L_2-Err	q	L_2-Err	q	L_2-Err	q
$41+11$	-0.96		-0.99		-0.94	
$81+21$	-1.60	3.45	-1.64	4.03	-1.63	2.95
$161+41$	-2.22	3.34	-2.26	3.55	-2.27	2.94
$321+81$	-2.82	3.15	-2.88	3.13	-2.89	2.97
$641+161$	-3.43	3.05	-3.48	3.03	-3.48	2.99

(c) sixth order accuracy

	BAN		BON		LDG	
Points	L_2-Err	q	L_2-Err	q	L_2-Err	q
$41+11$	-1.45		-1.34		-1.33	
$81+21$	-2.62	3.97	-2.65	4.37	-2.18	2.83
$161+41$	-3.81	4.04	-3.86	4.03	-3.27	3.62
$321+81$	-5.05	4.13	-5.06	3.97	-4.47	3.98
$641+161$	-6.26	4.04	-6.26	3.99	-5.68	4.03

Table 8: Grid convergence rate with non-compact form in two subdomains of nonuniform mesh.

So far we have used the non-compact form. Table 9 shows the convergence q for the BAN and BON schemes on compact form. In Table 9 the convergence rate for the second and fourth order accurate schemes are in line with the theoretical conclusion in Table 5. Note that the convergence rates using the sixth order scheme in Table 9 attain almost 6 while the theoretical value is 5.

(a) second order accuracy

	BAC		BOC	
Points	L_2-Err	q	L_2-Err	q
41	−1.07		−1.07	
81	−1.68	2.02	−1.69	2.12
161	−2.29	2.02	−2.29	2.01
321	−2.89	2.00	−2.89	2.00
641	−3.50	2.00	−3.49	2.01

(b) fourth order accuracy

	BAC		BOC	
Points	L_2-Err	q	L_2-Err	q
41	−2.21		−1.85	
81	−3.27	3.58	−2.84	3.36
161	−4.38	3.73	−4.30	4.88
321	−5.57	3.97	−5.54	4.14
641	−6.81	4.12	−6.79	4.16

(c) sixth order accuracy

	BAC		BOC	
Points	L_2-Err	q	L_2-Err	q
41	−2.35		−2.37	
81	−3.77	4.89	−3.79	4.89
161	−5.34	5.30	−5.35	5.28
321	−7.04	5.70	−7.04	5.69
641	−8.83	5.70	−8.82	5.95

Table 9: Grid convergence of approximations of $u_t + u_x = 0.01u_{xx}$ on two subdomains of non-uniform mesh in $[-1, 1]$.

5.3 The reflexion properties

To test the reflexion and oscillation properties of these schemes, a "wave" like analytic solution of (1) is chosen

$$u = \kappa \exp(-\theta(x - ct + b)^2). \tag{39}$$

The initial data, boundary data and forcing function are modified to adapt to the analytic solution (39). The forcing function in (1) becomes

$$F = -\varepsilon\big(- 2\kappa\theta + 4\kappa\theta^2(x - ct + b)^2\big) \exp\big(- \theta(x - ct + b)^2\big) \tag{40}$$

In all tests we use $a = 1$, $\varepsilon = 0.01$, $\kappa = 0.5$, $\theta = 100$, $b = 0.8$ and $c = 1$. The exact solutions at $T = 0.3$, $T = 0.8$ and $T = 1.3$ are shown in Figure 2. With increasing time, the solution propagate from left to right without changing form.

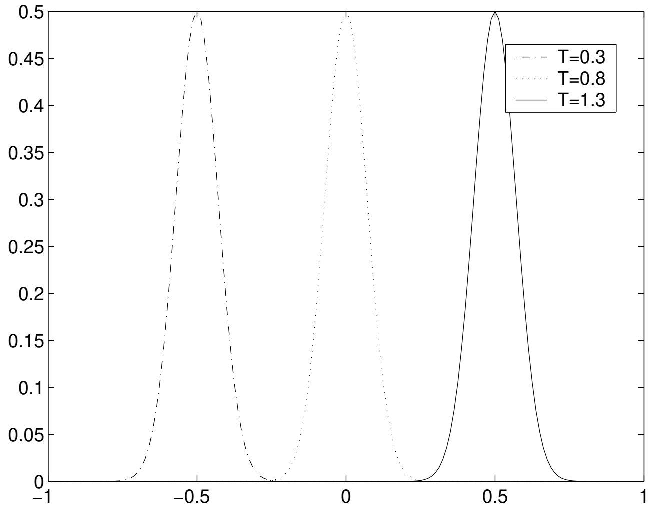

Figure 2: Exact solution.

The error of the schemes are presented at $T = 0.3$, $T = 0.8$ and $T = 1.3$ in Figures 3 and 4. We notice that for the SIN scheme (without an interface), the error propagate from left to right. In both second order accurate case (see Figures 3) and sixth order accurate case (see Figures 4), the error propagate from left to right via the interface at $x = 0$ without reflexion and oscillation for all compact schemes. However the schemes BAN, BON and LDG (with non-compact form) lead to an oscillation of the error caused by the interface. The oscillation of the error attains a maximum when the "wave" pass the interface around $T = 0.8$ (see Figures 4). But is also clearly seen propagating backwards at $T = 0.8$. The schemes BAC and BOC (with compact form) also introduces an oscillation at interface, however the magnitude of the oscillation is very small compared with the non-compact schemes.

Sixth order accurate dissipation operators [12] are introduced in the non-compact schemes BAN, BON and LDG. The calculations are shown in Figure 5. By comparing with the calculations in Figure 4 we find that the artifical dissipation operators kill the non-physical numerical oscillations efficiently for schemes BAN and BON. However the artificial dissipation only reduce the magnitude of the oscillation of LDG to 30%.

6 Conclusions

Stable and accurate interface treatments for the linear advection-diffusion equation have been studied. The treatments are based on SBP method and SAT technique, which lead to an energy estimate and stability. Accurate high order calculation are achieved in both single domain and multiple domains with an interface.

Three stable interface procedures–the Baumann-Oden method, the "borrowing" method and the local discontinuous Galerkin method have been investigated. The spectral radius for the schemes depend on the chosen coefficients. We can always find optimized coefficients to reduce the spectral radius. Specially, when the centered fluxes is used in the LDG, the minimal spectral radius has been obtained.

The compact form and non-compact form of the second derivative SBP operators have been compared. By using the compact form we can obtain one order higher accuracy than the non-compact form. Moreover, the compact form introduces less reflection and oscillation than the non-compact form. The artificial dissipation can reduce the non-physical oscillation from the interface for the non-compact form.

In short, this analysis show that only minor differences separates the different interface procedures. However the local discontinuous Galerkin method is more difficult to implement since the scheme requires one to rewrite the original viscous problem as a first order system of equations.

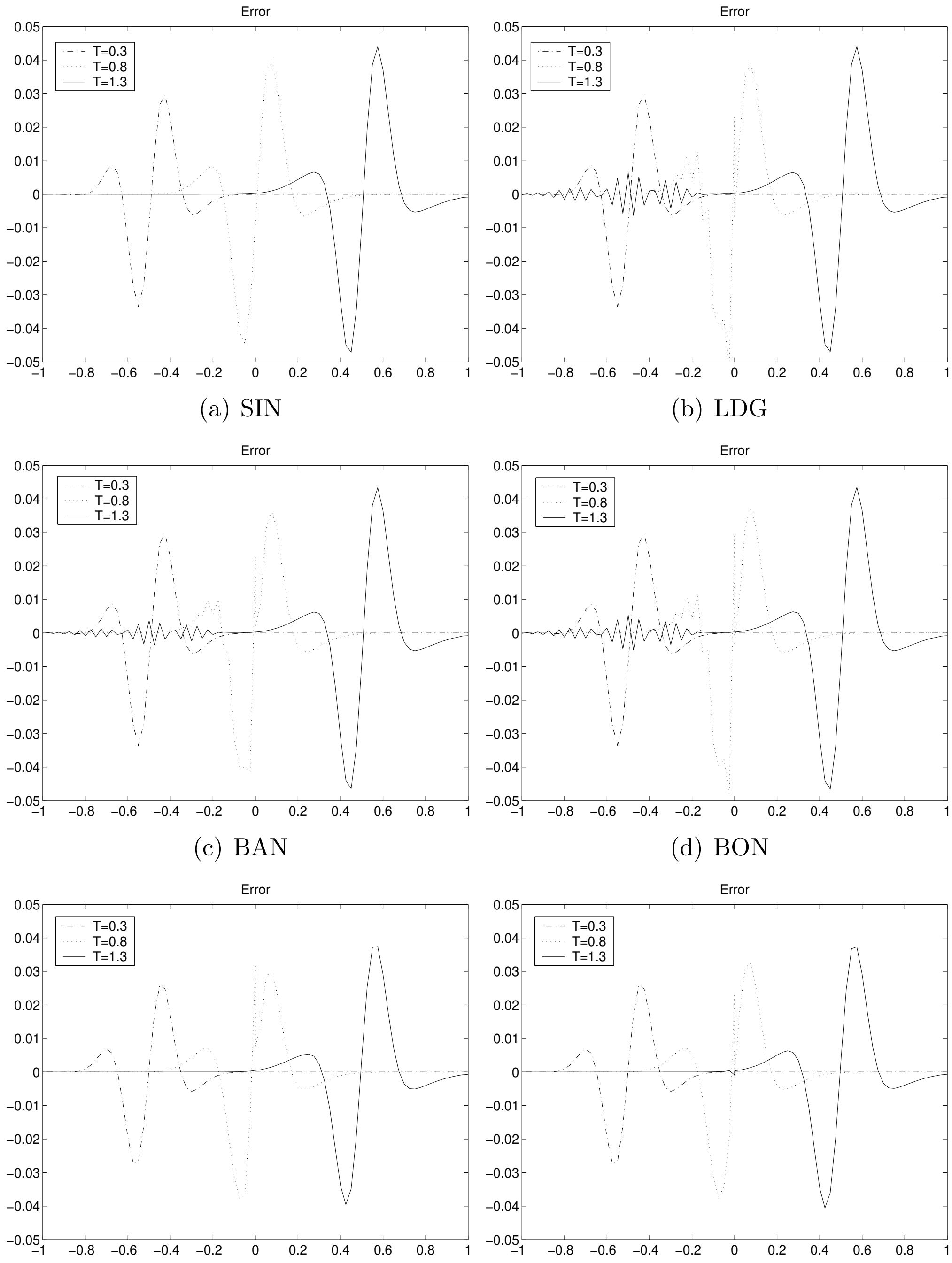

(a) SIN

(b) LDG

(c) BAN

(d) BON

(e) BAC

(f) BOC

Figure 3: Error. Second order accuracy. 81 points used. $\sigma_2^L = -\varepsilon/2$.

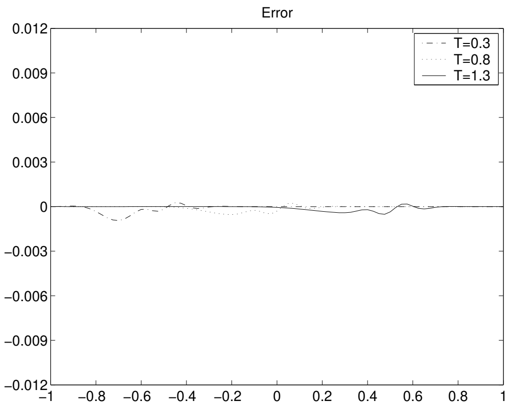

(a) SIN

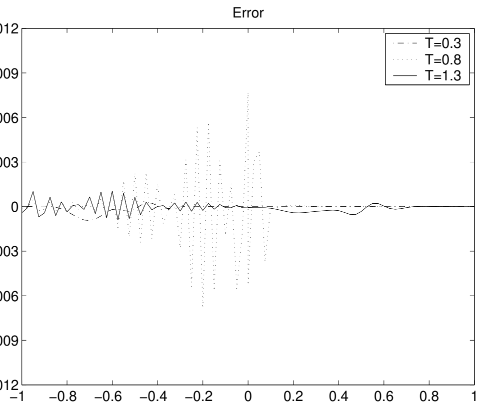

(b) LDG

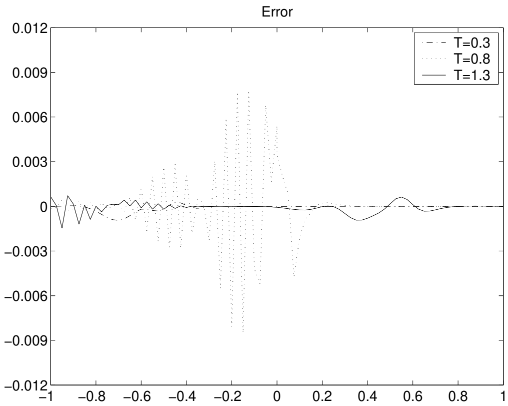

(c) BAN

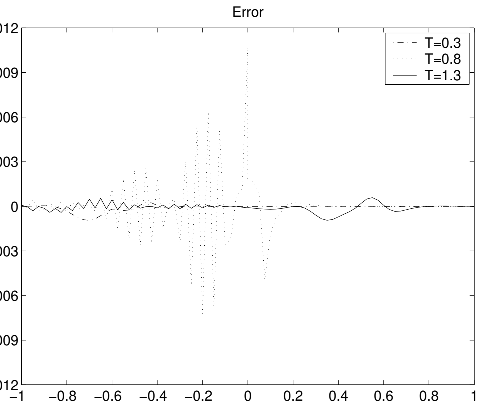

(d) BON

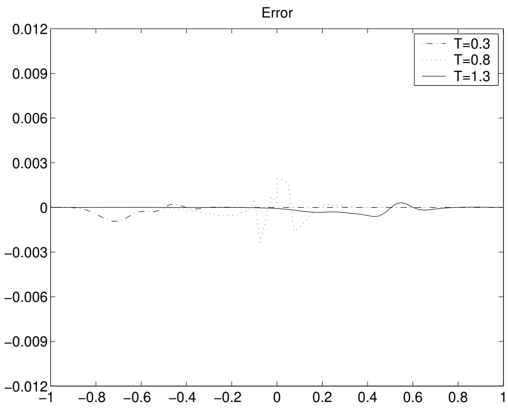

(e) BAC

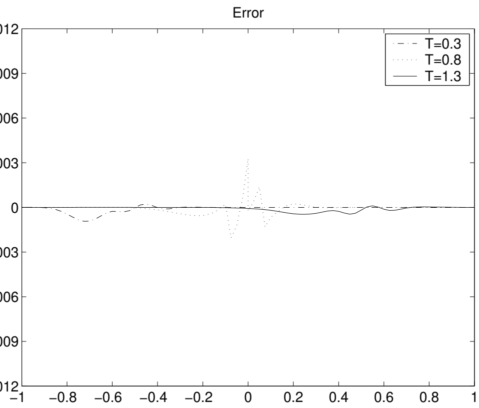

(f) BOC

Figure 4: Error. Sixth order accuracy. 81 points used. $\sigma_2^L = -\varepsilon/2$.

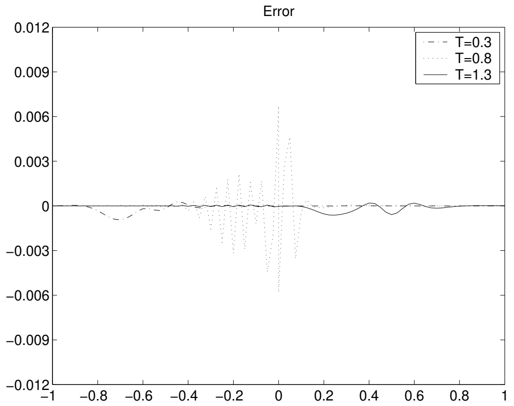

(a) LDG

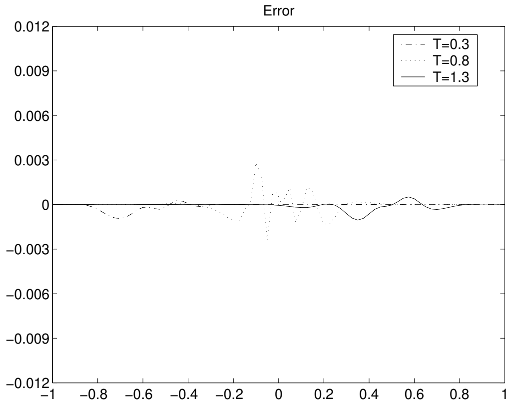

(b) BAN

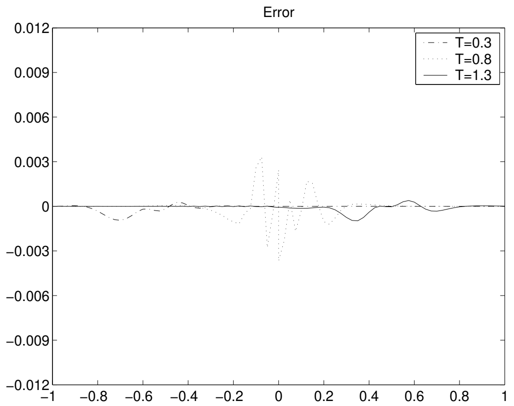

(c) BON

Figure 5: Error. Sixth order accuracy with the artificial dissipation operators. 81 points used. $\sigma_2^L = -\varepsilon/2$.

Appendix

Here we prove Lemma 4.1.

When $s \le -a^2/(4\varepsilon)$, $s \in \Re$, the term $\sqrt{1 + 4s\varepsilon/a^2}$ is a pure imaginary number and $\kappa_{1,2}$ becomes

$$\kappa_{1,2} = \frac{a}{2\varepsilon}\left(1 \pm \sqrt{1 + \frac{4s\varepsilon}{a^2}}\right) = c(1 \pm b(s)i)$$

where $c = a/(2\varepsilon) > 0 \in \Re$ is a constant and $b(s) = \left|\sqrt{-(1 + 4s\varepsilon/a^2)}\right| \ge 0 \in \Re$. Substituting $\kappa_{1,2}$ into (36) yields

$$\begin{aligned}
\det C(s) &= \big[1 + \beta c(1 - b(s)i)\big]c(1 + b(s)i)e^{c(1+b(s)i)} \\
&\quad - \big[1 + \beta c(1 + b(s)i)\big]c(1 - b(s)i)e^{c(1-b(s)i)} \\
&= 2ce^c\big[b(s)\cos(cb(s)) + (1 + \beta c + \beta c b^2(s))\sin(cb(s))\big]i \\
&= F(b(s))i
\end{aligned} \tag{41}$$

which only contains imaginary parts and the continuous real-function

$$F(b(s)) = 2ce^c\big[b(s)\cos(cb(s)) + (1 + \beta c + \beta c b^2(s))\sin(cb(s))\big], \qquad F(b(s)) \in \Re.$$

We have

$$\begin{aligned}
F\Big(b(s) = \frac{2n\pi}{c}\Big) &= 2ce^c\frac{2n\pi}{c} = 4ne^c\pi > 0, \\
F\Big(b(s) = \frac{(2n+1)\pi}{c}\Big) &= -2ce^c\frac{2n\pi}{c} = -4ne^c\pi < 0. \qquad n = 1, 2, \dots
\end{aligned} \tag{42}$$

As a result, there exists $b(s) \in [2n\pi/c, (2n+1)\pi/c]$ or

$$s = -\frac{a^2(b^2+1)}{4\varepsilon} \in \Big[-\frac{a^2((2n+1)\pi + c^2)}{4\varepsilon c^2}, -\frac{a^2(2n\pi + c^2)}{4\varepsilon c^2}\Big], \qquad n = 1, 2, \dots,$$

such that $F(b(s)) = 0$. Therefore, (36) has a solution for $s \le -a^2/(4\varepsilon)$, $s \in \Re$.

However, we note that when $s > -a^2/(4\varepsilon)$, $s \in \Re$, the equation (36) has no solution. To verify this, we rewrite the term $\kappa_{1,2}$,

$$\kappa_{1,2} = \frac{a}{2\varepsilon}\left(1 \pm \sqrt{1 + \frac{4s\varepsilon}{a^2}}\right) = c(1 \pm b(s))$$

where $b(s) = |\sqrt{1 + 4s\varepsilon/a^2}| > 0$, $b(s) \in \Re$.

Applying $\kappa_{1,2}$ to (36) leads to

$$
\begin{aligned}
\det C(s) &= \left[1+\beta c(1-b(s))\right] c(1+b(s)) e^{c(1+b(s))} \\
&\quad - \left[1+\beta c(1+b(s))\right] c(1-b(s)) e^{c(1-b(s))} \\
&= c e^{c(1-b(s))} \left[e^{2cb(s)}(1+b(s)+\beta c-\beta c b^2(s)) - (1-b(s)+\beta c-\beta c b^2(s)) \right]
\end{aligned}
$$

The inequality derived from the well-posedness condition (3),

$$-1 \le \beta c \le 0,$$

implies that the term $1+b(s)+\beta c-\beta c b^2(s)$ is positive. Consequently we have

$$
\begin{aligned}
\det C(s) > & c e^{c(1-b(s))} \left[(1+b(s)+\beta c-\beta c b^2(s)) - (1-b(s)+\beta c-\beta c b^2(s))\right] \\
= & 2 c e^{c(1-b(s))} b(s) > 0
\end{aligned}
\tag{43}
$$

Therefore, $\det C(s)$ is always positive for $s > -a^2/(4\varepsilon)$, $s \in \Re$. ■

References

[1] C.E. Baumann and J.T. Oden. A discontinuous hp finite element method for convection-diffusion problems. *Computer Methods in Applied Mechanics and Engineering*, 175:331–341, 1999.

[2] M.H. Carpenter, D. Gottlieb, and S. Abarbanel. Time-stable Boundary Conditions for Finite-difference Schemes Solving Hyperbolic Systems: Methodology and Application to High-order Compact Schemes. *Journal of Computational Physics*, 111(2):220–236, 1994.

[3] M.H. Carpenter, J. Nordström, and D. Gottlieb. A Stable and Conservative Interface Treatment of Arbitrary Spatial Accuracy. *Journal of Computational Physics*, 148:341–365, 1999.

[4] B. Cockburn and C.-W. Shu. The local discontinuous galerkin method for time-dependent convection-diffusion systems. *SIAM Journal of Numerical Analysis*, 35:2440–2463, 1998.

[5] B. Gustafsson. The convergence rate for difference approximation to mixed initial boundary value problems. *Mathematics of Computation*, 29, 1975.

[6] B. Gustafsson. The convergence rate for difference approximation to general mixed initial boundary value problems. *SIAM Journal on Numerical Analysis*, 18(2):179–190, 1981.

[7] B. Gustafsson, H.-O. Kreiss, and J. Oliger. *Time Dependent Problems and Difference Methods*. John Wiley & Sons, Inc., 1995.

[8] H.-O. Kreiss and G. Scherer. *Finite element and finite difference methods for hyperbolic partial differential equations, in: C. De Boor (Ed.), Mathematical Aspects of Finite Elements in Partial Differential Equation*. Academic Press, New York, 1974.

[9] K. Mattsson. Boundary Procedures for Summation-by-Parts Operators. *Journal of Scientific Computing*, 18(1):133–153, 2003.

[10] K. Mattsson. *Summation-by-Parts Operators for High Order Finite Difference Methods*. Phd thesis, Uppsala University, Depart. of Scientific Computing, Uppsala Univ., Uppsala, Sweden, 2003.

[11] K. Mattsson and J. Nordström. Summation by Parts Operators for Finite Difference Approximations of Second Derivatives. *Journal of Computational Physics*, 199:503–540, 2004.

[12] K. Mattsson, M. Svärd, and J. Nordström. Stable and Accurate Artificial Dissipation. *Journal of Scientific Computing*, 21(1):57–79, 2004.

[13] J. Nordström and M. H. Carpenter. High-order Finite Difference Methods, Multidimensional Linear Problems and Curvilinear Coordinates. *Journal of Computational Physics*, 173:149–174, 2001.

[14] J. Nordström, K. Forsberg, C. Adamsson, and P. Eliasson. Finite Volume Methods, Unstructured Meshes and Strict Stability. *Applied Numerical Mathematics*, 45:453–473, 2003.

[15] J. Nordström and R. Gustafsson. High Order Finite Difference Approximations of Electromagnetic Wave Propagation Close to Material Discontinuities. *Journal of Scientific Computing*, 18(2):215–234, 2003.

[16] J. Nordström and J. Gong. A Stable and Efficient Hybrid Method for Aeroacoustic Sound Generation and Propagation. *Comptes Rendus Mecanique*, 333:713–718, 2005.

[17] J. Nordström and J. Gong. A Stable Hybrid Method for Hyperbolic Problems. *Journal of Computational Physics*, 212:436–453, 2006.

[18] W.H. Reed and T. R. Hill. Triangular mesh methods for the neutron transport equation. Technical Report LA-UR-73-479, Los Alamos Scientific Laboratory, 1973.

[19] C.-W. Shu. Different formulations of the discontinuous galerkin method for the viscous terms. In Z.-C. Shi, M. Mu, W. Xue, and J. Zou, editors, *Advances in Scientific Computing*. Science Press, 2001.

[20] B. Strand. Summation by parts for finite difference approximation for d/dx. *Journal of Computational Physic*, 110(1):47–67, 1994.

[21] B. Strand. Numerical studies of hyperbolic IBVP with high-order finite difference operators satisfying a summation by parts rule. *Applied Numerical Mathematics*, 26(4):497–521, 1998.

[22] M. Svärd, K. Mattsson, and J. Nordström. Steady-Stable Computations Using Summation-by-Parts Operators. *Journal of Scientific Computing*, 24(1):79–95, 2005.

[23] M. Svärd and J. Nordström. On the Order of Accuracy for Difference Approximations of Initial-Boundary Value Problems. *Accepted in Journal of Computational Physics.*